



**Acoustics'08
Paris**
June 29-July 4, 2008
www.acoustics08-paris.org

Quantitative Ultrasonics for Inclusion and Pore Characterization of Steel Billets

Ville Kananen^a, Joonas Eskelinen^a and Edward Hægström^b

^aUniv. of Helsinki / Dept. of Physical Sciences, POB 64 (Gustaf Hällströmin katu 2), 00014
Helsinki, Finland

^bElectronics Research Unit, University of Helsinki, P.O.Box 64 (Gustaf Hällströmin katu 2),
FIN-00014 Helsinki, Finland
ville.kananen@helsinki.fi

We present a quantitative study on ultrasonic inclusion and pore classification in ball bearing steel 100Cr6. A 10.5 MHz focused transducer (14cm focal length in water, 76% -6 dB relative bandwidth) was scanned across the top surface of immersed 22*12*6cm³ production samples (8pcs) in pulse-echo mode. Automated pre-processing was employed to detect inclusions in samples. Wavelet transform and cross-correlation were applied to the back-scattered RF-signals of identified inclusions and pores. This allowed characterizing the shape of the echo signals from wavelet coefficients (WC) and cross-correlation coefficients: the echo is a superposition of the reflection from the inclusion front and back surface, whereas pores exhibit no back surface echo due to their large acoustic impedance mismatch. The echo frequency content was analyzed by short-time Fourier transform. Differences in echo characteristics between different inclusion and pore classes allow quantitative inclusion and pore characterization. We discriminate three classes: oxide-inclusions (aluminium-oxides), sulphides (manganese-sulphide), and sulphide-inclusion ensembles comprising oxide-inclusions in rolled steel samples (reduction ratio 10). Classification probability estimates with corresponding statistical relevance analysis are presented. We also estimate the inclusion shape, position, and orientation.

1 Introduction

Ultrasonic non-destructive testing (NDT) is one of the many steel inspection techniques which possess advantages compared to destructive methods [1]. Destructive methods, like macrographic examination by sulphur print (Baumann method), blue fracture testing, and step-down testing, are widely used in the steel industry for inclusion content estimation of steel products [2]. Combined with destructive sample preparation these techniques allow characterizing smaller volumes than the ultrasonic method. Ultrasound is widely used in the steel industry for quality control to count and to size inclusions and pores in steel samples [3, 4]. When large inclusions/pores (FBs) are identified, the sample is cut and the inclusions and pores are analyzed using a scanning electron microscope (SEM) to determine the content of the inclusions. SEM images allow estimating whether the inclusions are harder or softer than the steel matrix. This information is used to determine whether the quality of the test sample's casting is high enough for end users. This kind of FB characterization is laborious (the sample is measured, cut, ground to find FB, and SEM imaged to clarify the inclusions' chemical composition). Hence there is a demand to develop non-destructive ultrasonic methods to ease FB characterization in steel billets.

Signal processing techniques, like wavelet transform (WT) and short-time Fourier transform (STFT) allow computational signal analysis for quantitative feature extraction from measured ultrasonic signals. Phase, frequency and amplitude of the ultrasonic echoes are influenced by the FB shape, size, orientation and material content. The continuous wavelet transform (CWT) has been used for quantitative FB characterization [5]. In the study of Tsui and Basir, steel and glass FBs were placed free on a convex shaped glass dish immersed in a water bath and ultrasonic echo signals reflected from them were analyzed using CWT. The method allowed characterizing mm-size FBs, by FB material and shape, with a classification probability exceeding 98%. This technique is also applicable for quantitative FB characterization in steel when the influence of small FBs on the ultrasonic echo is considered (Rayleigh scattering regime). Römer employed the discrete wavelet transform (DWT) to discriminate oxide inclusions from pores [6]. The classification results for regular (non-alloyed) steels were close to the ones expected from metallurgical knowledge of the inclusion material

discovered from this steel grade. For ball bearing steel (alloyed steel), however, the results were not in accordance with the metallurgical knowledge. The efficiency of the CWT to analyze dispersive elastic waves propagating in a steel cylinder was studied by Kim and Kim [7]. The CWT and STFT performance was compared in terms of their time-frequency capability to analyze waves generated by an impacting solid circular cylinder. CWT outperforms the STFT when time-resolution at high frequencies rather than at low frequencies is desirable. Darmon, *et al.* modeled the ultrasonic response of alumina inclusions in steel [8]. They used a modified Born approximation which assumes that the wave pressure inside the scattering FB equals the unperturbed incident wave pressure for both weak and strong scattering inclusions. This model can deal with various inclusion shapes and was selected and implemented into the CIVA (French Atomic Energy Commission (CEA), France) simulation software. Better than 3 dB agreement in first echo amplitude between the simulated data and measured data was obtained.

Our aim was to develop an ultrasonic method for quantitative inclusion and pore characterization of ball bearing steel samples. An existing ultrasonic instrument in Ovako Bar ltd. (Imatra, Finland) was used for the steel sample measurements. The CWT was chosen for analysis due to its promising FB classification results presented in the study of Tsui and Basir [5]. Due to the increasing time-resolution as a function of frequency, the CWT should be a powerful method for quantitative FB classification. STFT was used to measure FB echo frequency components locally in this study [7]. Due to the minimum time-bandwidth product a Gaussian window was chosen for STFT [9]. Finally, normalized cross-correlation (CC) coefficients between the measured FB echoes were calculated to detect similarities in signals' phase and shape [10]. Results from three oxide-inclusions, four sulphide-inclusions, and six Sulphide-inclusion lines comprising oxide-inclusions were obtained.

2 Methods

2.1 Samples

Eight 100Cr6 ball bearing steel samples were taken from a 36x38 cm² bloom and rolled into six 9 cm diameter and two 11 cm diameter steel samples. The over 20 cm long samples were exposed to heat-treatment for almost a day. The

treatment comprised a controlled heating and cooling of the solid state sample to smooth its grain structure and to reduce inhomogeneities in the sample. Then the samples were cut and cropped into six 4 cm thick and two 6 cm thick steel samples featuring flat top and bottom surfaces, see Fig 1. These samples were analyzed ultrasonically for inclusions and pores. The ultrasonic results were verified by cutting the measured steel samples and by grinding the cut samples at 0.5 mm steps to find inclusions/pores by means of optical images. The FB class (oxide-inclusion, sulphide-inclusion, or pore) of each investigated inclusion was verified by optical microscopy.

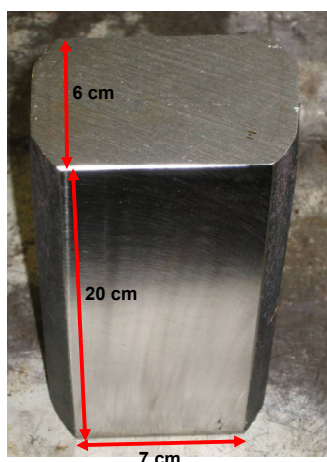


Fig.1 Steel sample.

2.2 Measurements

The ultrasonic instrument (Fig. 2) featured an ultrasonic immersion transducer (Krautkramer 10.5 MHz, 76% -6 dB relative bandwidth) driven by pulser/receiver card (AD-IPR-1210, NDT Automation, Princeton, USA) installed into a computer. The stepper motor and motion control board was SMC-4 (NDT Automation, Princeton). A Physical Acoustics (Acoustic Emission, Non-Destructive Testing Systems, Cambridge, UK) UltraWin (ver. E2.84) was used as the measurement software. A 320 V negative spike excitation and a pulse repetition frequency (PRF) of 1.2 kHz with no filters were used on the transmission side. The received signal was amplified 54 dB and band pass filtered (0.5-30 MHz). No averaging was used.

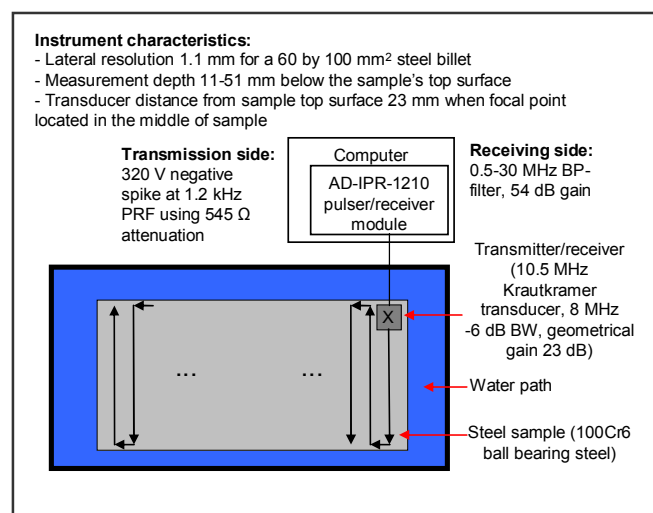


Fig.2 Measurement schematics.

Amplitude data and time-of-flight (TOF) data were measured locally (pixel-by-pixel) from the ultrasonic signals reflected inside the steel sample. The signals were time windowed to depths 13-36 mm in 4 cm thick samples and 11-51 mm in 6 cm thick samples below the sample surfaces. The highest echo amplitudes inside the steel sample of each A-line (one pixel) were used as reference amplitude values. The TOF values were calculated from the highest echo amplitude locations. The RF-signals were stored in the computer memory for off-line signal processing.

The steel samples were first scanned (150 mm/s) across the samples' top and bottom surfaces (pulse-echo measurement) at 0.25 mm step length to locate FBs in the sample. FB location, shape, orientation, and size together with metallurgical knowledge of FB characteristics were used to select the interesting FBs. Single pores are circular or ellipsoidal-shaped and located in the middle of sample, whereas sulfides and oxides are located closer the sample's surfaces and appear as line-shaped scatterer ensembles or individual FBs.

Chosen FBs were scanned second time (5 mm/s) at 50 μm step length to measure FB shape, orientation, and location more accurately. The transducer focal point was set on the FB location to maximize the SNR and to be able to use plane wave approximation in the signal processing. The scans from both sides of the sample allowed estimating the FB or FB ensemble thickness within the limit of the instrument axial resolution (300 μm).

2.3 Signal processing

The inclusion characterization software was programmed with MATLAB v. 7.4 for quantitative steel billet inclusion and pore classification using the CWT, STFT, and cross-correlation techniques. Cubic data interpolation was used to up-sample the received signal by a factor of four to decrease the quantization error generated by the 100 MHz sampling rate. To maximize the SNR, the reflected signals from the centre of each FB on the xy-scan plane were analyzed. These planes were chosen because at these points the maximum amplitude echo from the FB is received. The distance-amplitude correction (DAC) and focal gain compensation (FGC) were carried out on the A-lines (RF-signals). For C-scan images, Hilbert transform was used to obtain the corrected RF-signals envelope and the amplitude values were converted into logarithmic scale using the maximum amplitude of the whole measured volume as a scaling factor. The dynamic range was selected based on the image maximum amplitude and background echo amplitudes.

To make the calculated WCs, STFT-coefficients and CC-coefficients comparable, the corrected signal amplitudes were normalized to 1 V. As a result large variations in echo amplitudes from different FBs don't cause large variations in the calculated WCs, STFT-coefficients and CC-coefficients. The RF-signals were aligned in the time domain using the first zero crossing point (positive to negative) of the first discernible peak as a reference point [5]. This was done to compensate for phase shifts smaller than the up-sampled sampling interval (2.5 ns). This procedure should improve the classification results by improving the calculated WC and STFT-coefficients' SNR. The procedure eliminates the phase difference between

different signals that bias the calculated WCs and STFT-coefficients by increasing the variation in same FB class' coefficients. This of course also biases the FB classification results and therefore the phase difference correction allows more accurate FB classification.

Due to the frequency dependence of attenuation, the high-frequency components attenuate stronger than low-frequency components [11]. Therefore, the measured FB echoes were corrected by the attenuation effect on the signals at the propagation path in the steel sample. This was done by multiplying the discrete Fourier transform coefficients by the inverse of the attenuation effect on the FB echo frequencies and finally taking the inverse discrete Fourier transform of the corrected spectrum. Frequency exponent 1.5 and sound attenuation 0.4 dB/cm at 10 MHz in steel were used. Due to the low sound attenuation in water, only attenuation correction inside the steel sample was done.

Signals from four known sulphide-inclusions, three known oxides, and three sulphide-inclusion ensembles, comprising oxide-inclusions were digitally processed off-line (MathWorks MATLAB 7.4). The inclusion material was verified by optical microscopy. FB location in the xy-plane from the sample edges was determined from the c-scan images whereas the FB depth from both surfaces was calculated as the product of the FB echo TOF and sound velocity in the sample (5900 m/s [12]) divided by two. The FB depth information allows more accurate inclusion size estimation in the x- and y-directions (sample surface plane) because the depth is independent of echo amplitude variations in different inclusion pixels. All the inclusion echo depths are of similar whereas the surrounding pixels' echo depths differ significantly from the inclusion depth. The amplitude values of the inclusion pixels decrease towards the inclusion boundaries making the inclusion edge detection less accurate compared to echo depth data due to low SNR. FB shape and orientation parallel to the xy-plane (scanning plane) was estimated from the c-scan images: each y-direction scan maximum amplitude location y-coordinate was estimated and line was fit into these points. FB orientation was then calculated as an angle between this fitted line and the steel sample x-direction surface. The FB width and height in the c-scan image were calculated as the -6 dB points from the FB maximum amplitude point. The FB primary axis and small axis ratio was then calculated by the ratio of these values. The ratio gives an estimate of FBs shape: the ratio 1 indicates the circular shape whereas in the other case the FB shape is ellipsoid or line-like.

The Symlet wavelet at scales 1-50 was used in CWT for quantitative inclusion/pore classification. This wavelet shape was chosen because it resembled the measured RF signal shapes and because the symlet-wavelet has increasing time resolution at high frequencies. The WC difference (contrast) between the three inclusion classes was calculated as the average difference between all inclusion classes' WCs. The error bars for WCs were calculated as the standard deviation of these classes' WCs. For STFT-coefficients, the local spectrum average values of each inclusion classes' were calculated. Local spectrum standard deviations were used as error bars. One randomly chosen sulphide-inclusion echo was chosen as a reference and CC-coefficients between the reference echo and other nine FB echoes were calculated, separately. Indexes and maximum correlation coefficients were then calculated for

FB classification accuracy estimation. FB classification accuracy for CWT, STFT, and CC were estimated using the one-way analysis of variance statistic (ANOVA) model and testing the null hypothesis *can two different class FBs be discriminated statistically*. If the p-value is less than 0.05 the null hypothesis is fulfilled. Even though the number of inclusions in different FB classes was small, the p-value gives a rough estimate for the classification probability.

3 Results/Discussion

3.1 FB characteristics

Figure 3 illustrates Sulphide FB amplitude data from the FB top surface. The highest SNR is 26 dB. Figure 4 represents the FB depth in the sample. FB location in the steel sample was $(x, y, z) = (122.8 \pm 0.5, 42.7 \pm 0.5, 17.5 \pm 0.3)$ mm. FB orientation along x-axis was $(0.3 \pm 0.1)^\circ$, when the primary-axis and secondary-axis ratio was 4.6 ± 0.7 . The FB shape is more line-like than ellipsoidal due to rolling process in y-direction (ratio 10).

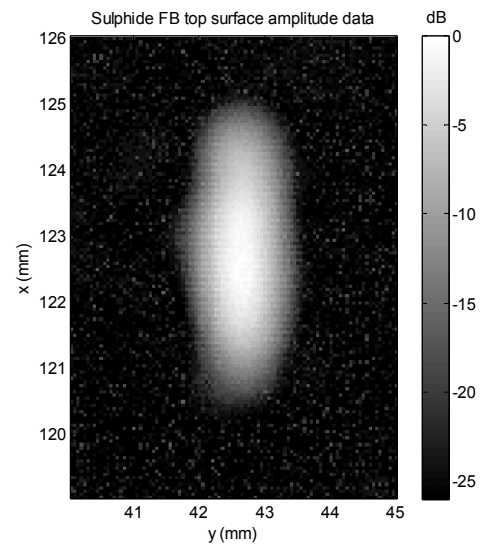


Fig.3 Sulphide FB top surface c-scan amplitude data.

Figures 5 and 6 represent the FB B-scans along the x- and y-axis. B-scan images allow FB orientation estimation along the z-axis (depth in the sample) and show all FBs along the sample depth, not only ones exploiting the highest echo amplitude as in the C-scan image. Figures 5 and 6 show that there are no other FBs before the FB of interest. This is necessary for successful quantitative measurement because scatterers in the ultrasonic wave propagation path affect the amplitude and the frequency spectrum of the signal.

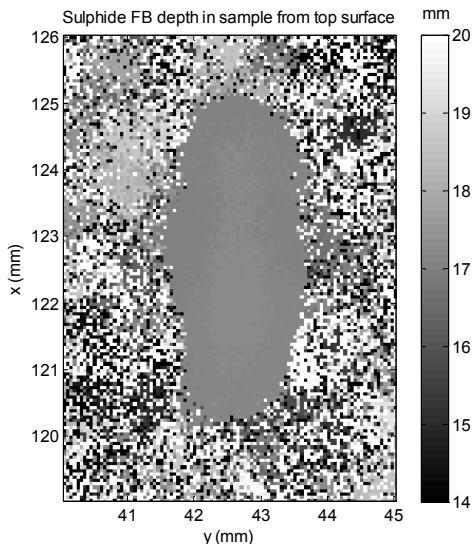


Fig.4 Sulphide FB depth in sample from top surface.

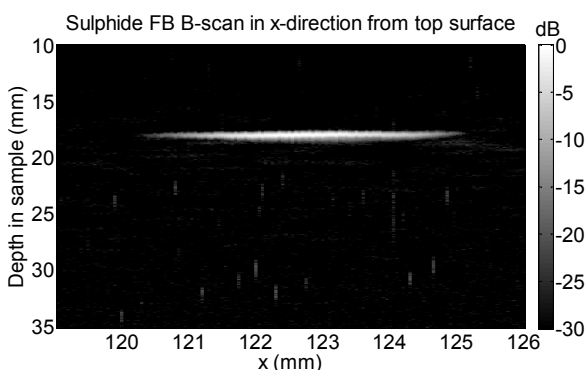


Fig.5 Sulphide FB B-scan in x-direction from top surface.

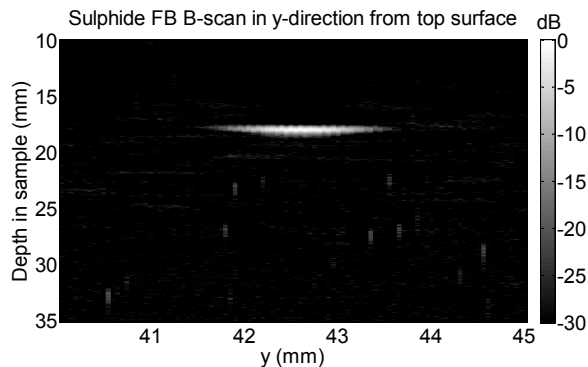


Fig.6 Sulphide FB B-scan in y-direction from top surface.

3.2 FB classification

Oxide FB, Sulphide FB, and Sulphide FB ensemble, comprising oxide inclusions echoes, CWT-coefficients, and STFT-coefficients are shown in figures 7, 8 and 9 as random examples. The oxide FB's 3rd and 4th peaks are small compared to the highest peak indicating the presence of small FB back wall reflections due to small acoustic impedance contrast between oxide FB and the steel matrix. The back wall echo arrives c.a. 50 ns after the front wall echo at inclusion size 200 μm . The sulphide FB's 2nd peak is small compared to oxide FB 2nd peak, whereas the 3rd and 4th peak are higher indicating high FB back wall echo arriving c.a. 200 ns later than the front wall echo for a 200 μm inclusion. The sulphide ensemble's echo is a superposition of all FBs' front wall echoes, echoes inside the FBs at sulphide-oxide boundaries, oxide-sulphide boundaries, and back wall echoes in the ultrasonic beam area.

A 0.2 μs long window with 87,5 % window overlap were used in the STFT. Back wall echoes are seen (3 dB amplitude) in the Sulphide FB and Sulphide FB ensemble STFT coefficients at 8.4 μs and 4.6 μs in 10-15 MHz frequency range.

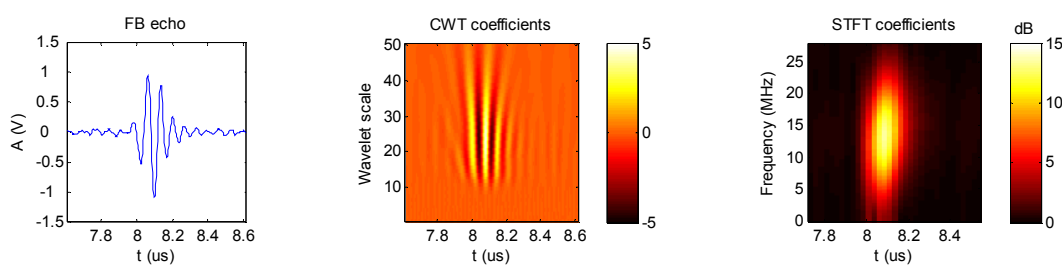


Fig.7 Oxide FB echo, CWT-coefficients (Symlet-12 wavelet) and STFT-coefficients.

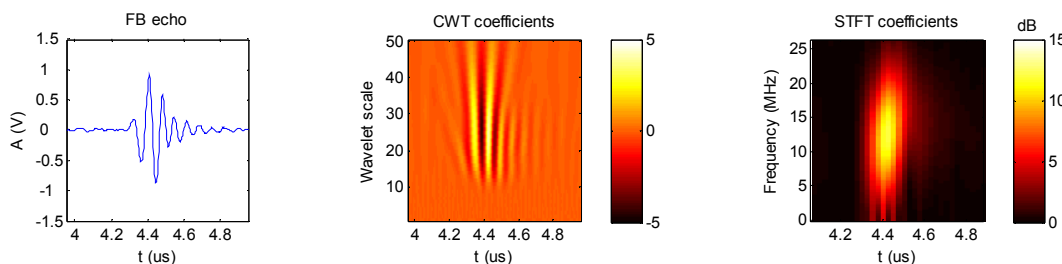


Fig.8 Sulphide FB echo, CWT-coefficients (Symlet-12 wavelet) and STFT-coefficients.

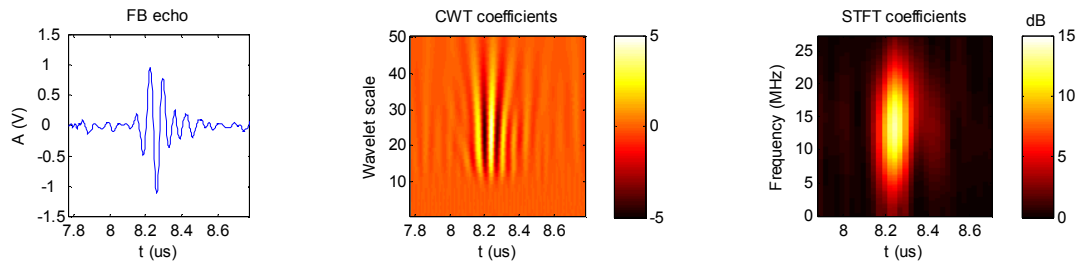


Fig.9 Sulphide ensemble FB echo, CWT-coefficients (Symlet-12 wavelet) and STFT-coefficients.

CWT, STFT, and CC were used to estimate the FB discrimination p-value for three Oxide FBs, four Sulphide FBs, and three Sulphide FB ensembles comprising oxide FBs. Results are shown in table 1. These results indicate that oxide FBs can be discriminated from sulphide FBs. The best method according to these measurements was CC coefficient maximum value whereas CWT was close to the limit (0.05) to be valid for FB classification. However, no valid method was found for sulphide FB discrimination from sulphide ensembles including oxide FBs.

FB discrimination p-values can be decreased by using more accurate corrections for the FB echoes. It is also important to verify the differences in the FB echoes and to understand what FB characteristics induce them. This provides detailed knowledge of sound-matter interaction in steel. Corrections of steel sample surface roughness as well as FB orientation, shape and size influences the FB echo amplitude, phase and frequency spectrum will be studied by means of numerical phantoms. This requires scattering theory implementation into the FB analysis.

	CWT	STFT	CC index	CC max corr. coeff.
p-value (oxides vs. sulphides)	0.0595	0.3	0.1276	0.0062
p-value (sulphides vs. Sulphide ensembles comprising oxides)	0.1231	0.1916	0.22	0.6027

Table 1 FB classification results

Acknowledgments

We thank M.Sc.(Tech) Ingmar Baarman from Ovako Wire Ltd. and Lic. Techn. Martti Veistaro and M.Sc.(Tech) Heikki Hurmola from Ovako Bar Ltd. for valuable guidance. We also thank Technical Adviser Tarja Hohti and M.Sc.(Tech) Ville Ruotsalainen from Ovako Bar Ltd. for helping with the ultrasonic instrument and steel sample analysis.

References

- [1] J. Krautkrämer, H. Krautkrämer, "Ultrasonic Testing of Materials", Third edition (1983), Springer-Verlag.
- [2] T. Hansén, P. G. Jönsson, "Some Ideas of Determining the Macro Inclusion Characteristics During Steelmaking", *Iron and Steel Society 2001 Electric Furnace Conference* (2001), Phoenix, Arizona, USA
- [3] T. Hansén, G. Runnsjö, K. Törresvoll, P. G. Jönsson, "On the Assessment of Macro Inclusions in Stainless Steels Using Ultrasonic Technique", *16th World Conference on Nondestructive Testing* (2004), Montréal, Canada
- [4] F. W. Margrave, K. Rigas, D. A. Bradley, P. Barrowcliffe, "The use of neural networks in ultrasonic flaw detection", *Measurement* 25, 143-154 (1999)
- [5] P. P. C. Tsui, O. A. Basir, "Wavelet basis selection and feature extraction for shift invariant ultrasound foreign body classification", *Ultrasonics* 45, 1-14 (2006)
- [6] S. Römer, "Discrimination of Ultrasonic Waves Reflected from Defects in Steels", Department of Mathematics (2003), Chalmers University of Technology / Göteborg University, Göteborg, Sweden
- [7] Y. Y. Kim, E.-H. Kim, "Effectiveness of the continuous wavelet transform in the analysis of some dispersive elastic waves", *Journal of Acoustical Society of America* 10, 86-94 (2001)
- [8] M. Darmon, P. Calmon, B. Bèle, "Modelling of the Ultrasonic Response of Inclusions in Steels", *Review of Quantitative Nondestructive Evaluation* 22, 101-108 (2003)
- [9] F. J. Harris, "On the Use of Windows for Harmonic Analysis with the Discrete Fourier Transform", *Proceedings of the IEEE* 66, 51-83 (1978)
- [10] J. C. Sarris, G. E. Cambourakis, "Subband Auto and Cross-Correlation Estimation by Recursive Filtering", *Proceedings of the 3rd International Symposium on Image and Signal Processing and Analysis*, Rome, Italy (2003)
- [11] G. S. Kino, "Acoustic Waves: Devices, Imaging, and Analog Signal Processing", Prentice-Hall Inc, 1-17 (2000)
- [12] G. S. Kino, "Acoustic Waves: Devices, Imaging, and Analog Signal Processing", Prentice-Hall Inc, 549-551 (2000)